BAREKENG: Journal of Mathematics and Its Applications
December 2026 Volume 20 Issue 4 Page 3369-3388
P-ISSN: 1978-7227 E-ISSN: 2615-3017
https://doi.org/10.30598/barekengvol20iss4pp3369-3388

SPATIO-TEMPORAL MODELING OF SEMI-HETEROSKEDASTIC RAINFALL DATA USING A GSTAR-GARCH FRAMEWORK

Nurhayati [1], **Muhammad Rozzaq Hamidi** [2], **Utriweni Mukhaiyar** [3*], **Kurnia Novita Sari** [4]

[1,2] *Doctoral Program in Mathematics, Faculty of Mathematics and Natural Sciences, Institut Teknologi Bandung*
[3,4] *Statistics Research Division, Faculty of Mathematics and Natural Sciences, Institut Teknologi Bandung*
Jln. Ganesha 10, Bandung, 40132, Indonesia

*Corresponding author's e-mail: ** **utriweni.mukhaiyar@itb.ac.id**

Article Info

Article History:
Received: 20th October 2025
Revised: 27th March 2026
Accepted: 02nd June 2026
Available online: 01st July 2026

Keywords:
Covariance matrix;
Heteroskedasticity;
Rainfall variability;
Spatial-dependence;
Volatility dynamics.

ABSTRACT

Rainfall often varies across time and space, with sudden and irregular changes that are difficult to capture. These variations are commonly linked to residual heteroskedasticity and spatial dependence, both of which can reduce the accuracy of statistical modeling when ignored. This study considers a semi-heteroskedastic setting, where residuals at one location remain stable while those at another show varying variance. To accommodate this mixed structure, we construct a covariance matrix that reflects both conditions. A hybrid model is then proposed by combining the Generalized Space-Time Autoregressive (GSTAR) framework with the Generalized Autoregressive Conditional Heteroskedasticity (GARCH) process. The GARCH component is used because it generalizes ARCH through a more flexible lag structure, allowing for better representation of volatility persistence and long-term fluctuations. The approach is applied to monthly average rainfall data retrieved from the NASA POWER database for two sites in Tasikmalaya Regency, Indonesia, which differ in distributional patterns and variability. The results show that the GSTAR-GARCH model can effectively capture spatial and temporal dependencies as well as volatility dynamics, performing consistently in both estimation and validation stages.

How to cite this article:

Nurhayati, M. R. Hamidi, U. Mukhaiyar and K. N. Sari., "SPATIO-TEMPORAL MODELING OF SEMI-HETEROSKEDASTIC RAINFALL DATA USING A GSTAR-GARCH FRAMEWORK", *BAREKENG: J. Math. & App.*, vol. 20, no. 4, pp. 3369-3388, Dec, 2026.

Journal homepage: *https://ojs3.unpatti.ac.id/index.php/barekeng/*
Journal e-mail: *barekeng.math@yahoo.com; barekeng.journal@mail.unpatti.ac.id*

Research Article · Open Access

1. INTRODUCTION

The GSTAR model not only accounts for the influence of past observations at the same location but also incorporates dependencies with neighboring locations [1], [2]. In data analysis, the temporal dimension typically highlights changes that occur over time [3], whereas spatial analysis emphasizes geographical relationships among objects or phenomena across locations [4]. Integrating these two approaches is therefore crucial for understanding phenomena that are simultaneously affected by spatial and temporal factors [5], [6]. To represent spatial dependence and variations in characteristics across locations, GSTAR employs a weight matrix [7], [8]. The selection of appropriate weights plays a major role in enhancing prediction accuracy [9], [10]. Nevertheless, GSTAR still assumes constant residual variance, whereas in reality, such variance can vary and exhibit instability across locations [11].

In the GSTAR framework, residual variance across locations may differ due to spatial dependence. Distinct local characteristics, such as microclimatic conditions, can influence residual fluctuations. Ignoring these characteristics may result in inefficient model estimation and potentially less accurate predictions [12]. Such inefficiency arises because the fundamental assumption of diagnostic tests, such as homoskedasticity, is violated, indicating that heteroskedastic effects remain present in the data [13]. To accommodate this condition, an approach that can dynamically capture changes in residual variance is required [14]. One such approach is the concept of volatility, defined as the degree of dispersion of a random variable over time and commonly measured using conditional variance [15], [16]. This concept has been widely applied in finance to explain data dispersion over time [17], [18], [19] and is equally relevant for modeling variance dynamics in rainfall data.

To more accurately represent the dynamics of residual variance, the Autoregressive Conditional Heteroskedasticity (ARCH) model introduced by [20] and its extension, the Generalized ARCH (GARCH) model by [21], can be employed as alternative approaches. These models assume that residual variance evolves over time in response to past squared residuals, thus providing a more flexible framework for modeling heteroskedastic patterns [22]. In the context of spatiotemporal data such as those modeled using GSTAR, the application of ARCH can enhance estimation efficiency and prediction accuracy by capturing both spatial and temporal variance fluctuations [23]. This approach is particularly important when residual variance cannot be assumed to be constant [24], as is frequently the case with rainfall data. Consequently, combining GSTAR with GARCH results in a GSTAR-GARCH framework that simultaneously represents spatiotemporal dependence and captures heteroskedastic dynamics in rainfall data.

Several previous studies have developed GSTAR models integrated with ARCH-based heteroskedasticity models to address non-constant residual variance. [25] developed GSTAR(1,1) with residual variance that accounts for heteroskedastic effects in the application of stock prices. [26] subsequently proposed GSTAR with ARCH effects and estimated the parameters using the maximum likelihood method. [14] introduced the GSTARI-X-ARCH model with the inclusion of exogenous variables and a data-mining approach to predict climate phenomena in West Java, allowing for more effective handling of big data. Furthermore, [27] developed GSTARIMA-ARCH for rainfall modeling in Java and demonstrated more accurate predictions compared with conventional models. In addition, [24] applied GSTARI-ARCH to inflation analysis in several cities in North Sumatra, using parameter estimation based on Generalized Least Squares (GLS). The application of GSTARI-ARCH was further extended by [28] for modeling Covid-19 positive case data in West Java and by [12] for predicting cyclone events in the United States. These studies highlight the considerable potential of integrating GSTAR and ARCH in modeling spatiotemporal data with heteroskedasticity. However, the limited flexibility of ARCH indicates the need for further development using more adaptive heteroskedasticity models such as GARCH.

Although numerous studies have successfully integrated GSTAR with ARCH models as described above, limitations remain regarding the flexibility of the heteroskedasticity modeling [29]. ARCH models tend to capture only short-term heteroskedastic effects and assume that variance depends entirely on past residual values [30]. As a result, they are less effective in representing long-lasting volatility or more complex heteroskedasticity patterns [21], [31]. In contrast, GARCH models offer a more flexible approach by incorporating lag effects of the variance itself, thus capturing more persistent and complex volatility dynamics [32]. Therefore, the development of a GSTAR model integrated with GARCH-based heteroskedasticity becomes essential to improve predictive performance and accuracy in spatiotemporal data modeling, particularly for phenomena with high volatility and dynamic changes, such as extreme rainfall.

This study addresses heteroskedasticity in the GSTAR framework by integrating a GARCH based conditional variance specification. Unlike previous GSTAR ARCH extensions, which restrict volatility dynamics to depend solely on past squared residuals, the proposed model incorporates location specific variance persistence through lagged conditional variances. The primary contribution lies in the formulation of a diagonal conditional covariance matrix with heterogeneous GARCH variance dynamics across spatial units. Under this specification, the model adopts a semi-heteroskedastic structure, allowing certain locations to exhibit conditional heteroskedasticity while others remain conditionally homoscedastic. Mathematically, the conditional covariance matrix is explicitly constructed as a diagonal matrix whose elements evolve according to location-specific GARCH recursions, while conditional cross-location covariances are constrained to zero. Consequently, heterogeneity arises from differences in variance persistence across spatial locations rather than from dynamic covariance interactions. The proposed formulation strictly generalizes the GSTAR-ARCH model as a nested special case when the variance persistence parameters are set to zero. Furthermore, the proposed specification differs from diagonal BEKK type formulations in its construction. Volatility evolves independently for each location and does not involve quadratic matrix recursions or dynamic cross location covariance interactions. From a multivariate volatility perspective, the GSTAR GARCH formulation can therefore be interpreted as a restricted diagonal representation of the BEKK framework. In this formulation, the conditional variance dynamics are integrated within the GSTAR mean structure through spatial weighting. Cross location variance correlations are intentionally excluded to maintain model parsimony. This yields a parsimonious yet mathematically explicit semi-heteroskedastic covariance structure that remains fully compatible with the spatial dependence specified in the GSTAR mean equation.

From a practical perspective, an improved characterization of rainfall volatility enhances risk assessment in Indonesia, particularly in detecting periods of extreme rainfall that may affect flood mitigation, agricultural planning, and water resource management. By jointly modeling spatial dependence and time-varying variance, the proposed framework captures not only mean rainfall dynamics but also volatility persistence across locations. These quantitative measures of conditional variance can serve as early indicators of heightened rainfall uncertainty and may be incorporated into forecasting and early warning systems. The remainder of this article is organized as follows. Section 2 presents the methodology, model specification, and construction procedure of the GSTAR-GARCH model. Section 3 describes the research data, the method for selecting the spatial weight matrix, parameter estimation, and model evaluation steps, including diagnostic testing and prediction validity assessment. Section 4 provides the conclusions and the key implications of the study.

2. RESEARCH METHODS

This study implements an analytical approach that integrates spatiotemporal modeling with volatility modeling. The initial stage begins with a descriptive analysis to identify general patterns in the rainfall data. Subsequently, the GSTAR model is applied to simultaneously capture spatial dependencies across locations and temporal dynamics. Once the spatiotemporal model is established, the analysis proceeds to the residuals to evaluate the presence of heteroskedastic effects. If the residual variance exhibits instability, ARCH or GARCH models are employed as a follow-up approach to model such volatility. This methodological framework is designed to account for both the mean pattern and the variance instability in the data. The overall analytical process is systematically illustrated in Fig. 1 in the form of a flowchart.

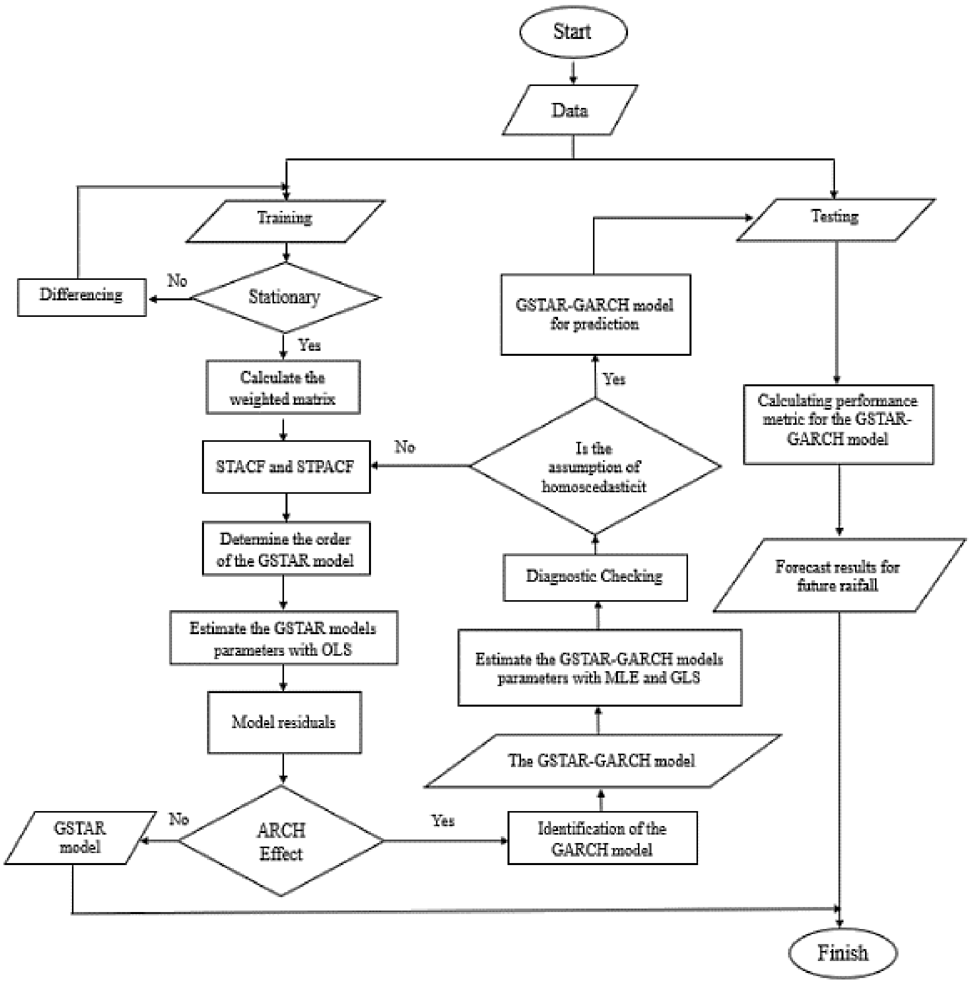

Figure 1. Research Flow Chart for Modeling and Forecasting Using GSTAR–GARCH Approach

2.1 The GSTAR Model

The GSTAR model was developed by [33] to simultaneously capture spatial and temporal dependencies. Unlike the Space-Time Autoregressive (STAR) model, which assumes uniform parameters across all regions, GSTAR allows parameters to vary at each observation point. This feature provides greater flexibility in representing spatial variation. The spatial structure is represented through a weight matrix that indicates the extent to which one location is influenced by other locations, while temporal relationships are captured through dependence on past values. This flexibility makes GSTAR well suited for modeling complex spatiotemporal phenomena that cannot be adequately addressed by classical time series models.

Let $\{Y_{i,t}\}$ be a mean-centered stochastic process at location $i = 1,2,\dots,N$ and time $t = p+1, p+2,\dots,T$. This process follows a GSTAR model of temporal order p and spatial orders $\lambda_1, \lambda_2,\dots, \lambda_p$, denoted as GSTAR($p$; $\lambda_1, \lambda_2,\dots, \lambda_p$), if it satisfies the following equation:

$$Y_{i,t} = \sum_{k=1}^{p}\left(\phi_{k0}^{(i)} Y_{i,t-k} + \sum_{l=1}^{\lambda_k} \phi_{k\ell}^{(i)} w_{ij}^{(\ell)}\, Y_{j,t-k}\right) + \varepsilon_{i,t} \tag{1}$$

where $\phi_{k0}^{(i)}$ and $\phi_{kl}^{(i)}$ are location-specific autoregressive parameters, and $w_{ij}^{(\ell)}$ denotes the (i, j)-th element of the spatial weight matrix $W^{(\ell)}$, which measures the influence of location j on location i at spatial order ℓ. In vector form, Eq. (1) can be written equivalently as:

$$\boldsymbol{Y}_t = \sum_{k=1}^{p}\left(\boldsymbol{\Phi}_{k0}\boldsymbol{Y}_{t-k} + \sum_{l=1}^{\lambda_k} \boldsymbol{\Phi}_{k\ell}\boldsymbol{W}^{(\ell)}\, \boldsymbol{Y}_{t-k}\right) + \boldsymbol{\varepsilon}_t, \tag{2}$$

where:

$\boldsymbol{Y}_t$: The observation vector at time t,

$\boldsymbol{\Phi}_{k0}$: The diagonal matrix of temporal autoregressive coefficients at lag k
$\boldsymbol{\Phi}_{k0} = \mathrm{diag}\left(\phi_{k0}^{(1)}, \phi_{k0}^{(2)}, \dots, \phi_{k0}^{(N)}\right)$,

$\boldsymbol{\Phi}_{kl}$: The diagonal matrix of spatial autoregressive coefficients at temporal lag k and spatial order ℓ
$\boldsymbol{\Phi}_{k\ell} = \mathrm{diag}\left(\phi_{k\ell}^{(1)}, \phi_{k\ell}^{(2)}, \dots, \phi_{k\ell}^{(N)}\right)$,

$\boldsymbol{W}^{(\ell)}$: The spatial weight matrix of order ℓ, $\boldsymbol{W}^{(\ell)} \in \mathbb{R}^{N\times N}$, with zero diagonal elements and row sums equal to one for $\ell > 0$, while $W^{(0)} = I_N$ denotes the identity matri,x

$\boldsymbol{\varepsilon}_t$: The vector of disturbance terms.

In the classical GSTAR framework, the disturbance vector $\boldsymbol{\varepsilon}_t$ is assumed to follow a multivariate normal distribution $\boldsymbol{\varepsilon}_t \sim \mathcal{N}(\mathbf{0}, \sigma^2 \boldsymbol{I}_N)$, where $\mathbf{0}$ is an $N \times 1$ zero vector, $\sigma^2 > 0$ is a scalar constant representing a common innovation variance across all locations and time, and I_N is an $N \times N$ identity matrix. This assumption implies homoskedasticity and contemporaneous independence across spatial locations, i.e., $\mathrm{Cov}(\varepsilon_{i,t}, \varepsilon_{j,t}) = 0$ for all $i \neq j$. While this assumption simplifies estimation and inference, it may be restrictive in applications where residual variance varies across locations or evolves over time. In the presence of heteroskedasticity, ignoring such variance dynamics may lead to inefficient parameter estimates and misleading inference. For this reason, the homoskedastic and uncorrelated disturbance assumption is relaxed in Section 2.3 through the introduction of a structured heteroskedastic covariance specification based on GARCH dynamics.

The GSTAR model has continued to evolve, both theoretically and in its applications across various fields. From a theoretical perspective, research has focused on strengthening stationarity properties through the Inverse Autocovariance Matrix approach [34], as well as developing new methods such as the kernel approach [35], [1], minimum spanning tree [23], [9], and the integration with kriging methods [36]. In addition, GSTAR has been studied in the context of correlated residuals [37], [38], the presence of outliers [39], [40], and discrete data [41]. Other studies have examined the invertibility of the kernel GSTAR model [42], the use of weight matrices such as Queen Contiguity [43], and comparisons of different types of weight matrices [44]. These developments demonstrate that GSTAR theory has not only advanced conceptually but has also continuously adapted to the increasing complexity of spatial and temporal data.

These theoretical advancements have laid the foundation for a wide range of GSTAR applications in practice. The model has been applied to diverse cases, including economic analysis [45], tea plantation yields [46], [38], palm oil production [47], and red chili commodity prices [48]. In the health sector, GSTAR has been used to analyze dengue fever cases [49] and Covid-19 spread [50], [23]. Other applications include crime prediction in Medan [37], air quality assessment [51], temperature variation analysis [52], coffee pest infestations [53], and rainfall prediction [10]. The model has also been utilized in peat soil studies [54], the distribution of copper and gold content [55], climate data modeling [56], [57], and forest fire prediction [58], [59]. These successful applications highlight the flexibility of GSTAR in handling a wide range of data types and real-world problems, reinforcing its relevance in both research and practice.

2.2 The ARCH and GARCH Model

In the conventional GSTAR model, residuals are assumed to follow a normal distribution with zero mean and constant variance (homoskedasticity). However, in practice, residual variance is often not constant and may change over time (heteroskedasticity). Ignoring this condition can lead to biased and inefficient parameter estimates. To address this issue, heteroskedastic models such as ARCH and GARCH are employed, as they are specifically designed to model time-varying residual variance. The ARCH model was first introduced by [20] to account for conditional variance, or volatility (h_t), in time series data. Subsequently, GARCH was developed by [21] as a more flexible version to capture volatility clustering. This model has become a standard approach in volatility analysis, particularly in the field of finance, and is now applied to enhance the GSTAR framework, allowing it to more accurately represent variance instability.

A process $\{\varepsilon_t\}$ is said to follow model if the conditional distribution of $\{\varepsilon_t\}$ given the available information, $\mathcal{F}_{t-1}$, up to $t-1$ time epoch can be represented as:

$$\varepsilon_t = \sqrt{h_t}\eta_t;\ \eta_t \sim N(0,1), \tag{3}$$

with $h_t = Var\,(\varepsilon_t|\mathcal{F}_{t-1})$ denoting the conditional variance (volatility) of ε_t given the information set available up to time $t-1$. The formula for h_t is derived from a stochastic heteroskedastic model. The term η_t refers to the innovation process, which is assumed to be independently and identically distributed (i.i.d.) with zero mean and unit variance [31]. The ARCH(1) model is one of the most basic models used to describe time-varying volatility. In this model, h_t is determined by the squared residual from the previous period. The mathematical form of h_t in the ARCH(1) model is given as follows:

$$h_t = \alpha_0 + \alpha_1 \varepsilon_{t-1}^2, \tag{4}$$

where $\alpha_0 > 0$ and $\alpha_1 \geq 0$. The parameter α_1 measures the short-term impact of shocks on volatility, and the condition $0 \leq \alpha_1 < 1$ ensures covariance stationarity. The ARCH model relies solely on past squared residuals. To capture persistent volatility patterns, a high order is required, which makes the model complex, computationally demanding, and potentially yields negative variance, thereby violating the non-negativity assumption [60]. The GARCH model addresses this limitation by incorporating past variances into the specification [21]. This structure allows GARCH to represent the gradual decay of volatility without introducing an excessive number of parameters. In a GARCH(1,1) model, conditional variance is defined as:

$$h_t = \alpha_0 + \alpha_1 \varepsilon_{t-1}^2 + \beta_1 h_{t-1}, \tag{5}$$

where $\alpha_0 > 0$, $\alpha_1 \geq 0$, and $\beta_1 \geq 0$. The model is weakly stationary if and only if $\alpha_1 + \beta_1 < 1$. In this specification, α_1 captures the short-run impact of shocks, while β_1 reflects the persistence of volatility over time. This univariate ARCH/GARCH framework serves as the fundamental building block for the multivariate and location-specific heteroskedastic structure introduced in Section 2.3, where conditional variance dynamics are extended to the spatio-temporal GSTAR setting.

2.3 The GSTAR - GARCH Model

This section explicitly constructs the proposed semi-heteroskedastic GSTAR–GARCH model by defining a diagonal conditional covariance matrix with location-specific GARCH variance dynamics. The construction formalizes how heterogeneity in conditional variance arises across spatial locations while maintaining zero conditional cross-location covariances under an explicit assumption of conditional independence. The GSTAR-GARCH model extends the conventional spatio-temporal autoregressive framework by incorporating a GARCH specification into the residual structure. This integration allows the model to jointly capture spatial interactions across locations, temporal dynamics, and volatility clustering within a unified specification. Unlike most existing studies that employ ARCH-type extensions and restrict the conditional variance to past squared residuals, the proposed GSTAR-GARCH formulation enhances the volatility dynamics by incorporating both lagged innovations and past conditional variances. Consequently, it provides a more flexible and robust framework for modeling complex spatio-temporal processes.

Formally, the GSTAR-GARCH model extends the GSTAR framework in Eq. (2) by allowing the residual variance to follow a GARCH process, as defined in Eq. (5). Within this framework, $\boldsymbol{\varepsilon}_t \in \mathbb{R}^{N\times 1}$ denotes the disturbance vector. These residuals are assumed to follow a multivariate normal distribution with covariance matrix $\boldsymbol{\Omega}_t = Var(\boldsymbol{\varepsilon}_t) \in \mathbb{R}^{N\times N}$. The proposed GSTAR($p$; λ_1, λ_2,…, λ_p) - GARCH(r, s) model is formulated as

$$\mathbf{Y}_t = \sum_{k=1}^{p} \left(\boldsymbol{\Phi}_{k0} \mathbf{Y}_{t-k} + \sum_{\ell=1}^{\lambda_k} \boldsymbol{\Phi}_{k\ell} \mathbf{W}^{(\ell)} \mathbf{Y}_{t-k} \right) + \mathbf{D}_t \boldsymbol{\eta}_t, \tag{6}$$

where $\mathbf{Y}_t = \left(Y_{1,t}, Y_{2,t}, \ldots, Y_{N,t}\right)' \in \mathbb{R}^{N\times 1}$ is the observation vector, and $\boldsymbol{\eta}_t \sim \mathcal{N}(\mathbf{0},\, \boldsymbol{I}_N)$ denotes standardized innovations of dimension $N \times 1$. The disturbance term is scaled by the diagonal scaling matrix $\mathbf{D}_t \in \mathbb{R}^{N\times N}$

$$\mathbf{D}_t = \operatorname{diag}\left(\sqrt{h_{1,t}}, \sqrt{h_{2,t}},\ \ldots, \sqrt{h_{N,t}}\right), \tag{7}$$

so that, element-wise,

$$\eta_{i,t} = \frac{\varepsilon_{i,t}}{\sqrt{h_{i,t}}}, i = 1,2, \ldots, N. \tag{8}$$

This formulation implies that each location has its own conditional variance $\mathrm{h}_{i,t}$, and the standardized innovation $\eta_{i,t}$ represents the residual normalized by this local volatility. This relation clarifies the role of conditional variance in standardizing each innovation. In this setting, $\varepsilon_{i,t}$ represents the raw disturbance at location i, while the collection $\boldsymbol{\varepsilon}_t = (\varepsilon_{1,t}, \varepsilon_{2,t}, \dots, \varepsilon_{N,t})'$ denotes the corresponding disturbance vector across all spatial locations. Here, $\mathbf{h}_t = \left(h_{1,t}, h_{2,t}, \dots, h_{N,t}\right)' \in \mathbb{R}^{N\times 1}$ denotes the vector of conditional variances, while $\mathrm{h}_{i,t}$ refers to its i-th element. The dynamics of $\mathbf{h}_t$ follow a multivariate GARCH recursion:

$$\mathbf{h}_t = \boldsymbol{\alpha}_0 + \sum_{m=1}^{r} \boldsymbol{\alpha}_m \odot \boldsymbol{\varepsilon}_{t-m}^{\odot 2} + \sum_{n=1}^{s} \boldsymbol{\beta}_n \odot \boldsymbol{h}_{t-n}, \tag{9}$$

with $\odot$ denoting the Hadamard (element-wise) product, where $\boldsymbol{\varepsilon}_{t-m}^{\odot 2} \in \mathbb{R}^{N\times 1}$ denotes the element-wise square of the residual vector, i.e., $\boldsymbol{\varepsilon}_{t-m}^{\odot 2} = (\varepsilon_{1,t-m}^2,\ \varepsilon_{2,t-m}^2, \dots, \varepsilon_{N,t-m}^2)'$. As an illustration, for the case $N = 3$, the Hadamard product can be written explicitly as

$$\boldsymbol{\alpha}_m \odot \boldsymbol{\varepsilon}_{t-m}^{\odot} = \begin{bmatrix} \alpha_{1,m} \\ \alpha_{2,m} \\ \alpha_{3,m} \end{bmatrix} \odot \begin{bmatrix} \varepsilon_{1,t-m}^2 \\ \varepsilon_{2,t-m}^2 \\ \varepsilon_{3,t-m}^2 \end{bmatrix} = \begin{bmatrix} \alpha_{1,m}\varepsilon_{1,t-m}^2 \\ \alpha_{2,m}\varepsilon_{2,t-m}^2 \\ \alpha_{3,m}\varepsilon_{3,t-m}^2 \end{bmatrix}.$$

This example clarifies that the Hadamard operator acts component-wise, contrasting with conventional matrix multiplication. This compact representation highlights the integration of spatio-temporal dependence (through $\boldsymbol{\Phi}_{k0}$, $\boldsymbol{\Phi}_{k\ell}$, and spatial weight matrices $\mathbf{W}^{(\ell)}$) with volatility dynamics (through the GARCH process of $\mathbf{h}_t$). From Eq. (7) and Eq. (8) the conditional covariance matrix of the error process is defined as

$$\boldsymbol{\Omega}_t = \mathrm{Var}(\boldsymbol{\varepsilon}_t \mid \mathcal{F}_{t-1}) = \boldsymbol{D}_t \boldsymbol{D}_t'. \tag{10}$$

Hence, the conditional covariance structure becomes

$$\boldsymbol{\Omega}_t = \mathrm{diag}(h_{1,t}, h_{2,t}, \dots, h_{N,t}), \tag{11}$$

so that

$$E(\varepsilon_{i,t}\varepsilon_{j,t} \mid \mathcal{F}_{t-1}) = \begin{cases} h_{i,t}, & i = j, \\ 0, & i \neq j. \end{cases} \tag{12}$$

This formulation implies that the proposed framework allows heterogeneous and time-varying conditional variances across spatial locations, while maintaining zero conditional cross-covariances. Therefore, the heterogeneity arises from differences in the conditional variance dynamics at each location rather than from cross-location covariance interactions. Mathematically, each variance component follows a univariate GARCH-type recursion,

$$h_{i,t} = \alpha_{i0} + \alpha_{i1}\varepsilon_{i,t-1}^2 + \beta_{i1} h_{i,t-1}, \tag{13}$$

so that volatility persistence and shock effects are modeled individually for each spatial unit. This structure extends the previously used GSTAR-ARCH specification, which is obtained as a special case when $\beta_{i1} = 0$ for all i. Consequently, the proposed model strictly generalizes the ARCH-based semi-heteroskedastic GSTAR framework by incorporating conditional variance persistence.

Comparatively, the proposed formulation is structurally distinct from diagonal BEKK type multivariate GARCH models. In the diagonal BEKK model introduced by Baba, Engle, Kraft, and Kroner, the conditional covariance matrix evolves through quadratic matrix recursions involving lagged covariance matrices and outer products of residual vectors. In contrast, the present framework constructs the conditional covariance matrix through independent location specific variance recursions and does not employ quadratic matrix updating mechanisms. The resulting difference therefore arises from the variance generation mechanism rather than from parameter restrictions alone. In summary, the novelty of the proposed semi heteroskedastic GSTAR framework lies in integrating spatial dependence in the mean structure with location specific persistent volatility processes. This formulation yields a diagonal yet heterogeneous conditional covariance structure that generalizes GARCH based GSTAR specifications. It can be interpreted as a restricted diagonal representation within the multivariate GARCH class under an explicit assumption of conditional independence across locations.

For the entire sample, residuals are stacked across both time and space into $\boldsymbol{\varepsilon} = (\boldsymbol{\varepsilon}_1, \boldsymbol{\varepsilon}_2, \dots, \boldsymbol{\varepsilon}_N)' \in \mathbb{R}^{N(T-p)\times 1}$, where $\boldsymbol{\varepsilon}_i \in \mathbb{R}^{N(T-p)\times 1}$ collects the residuals of location i from $t = p+1$ to $t = T$. The corresponding covariance matrix expands to $\boldsymbol{\Omega}_t \in N(T-p) \times N(T-p)$, whose diagonal structure depends on the assumed heteroskedasticity pattern. Specifically, (i) under homoskedasticity, the variance is constant across locations and time; (ii) under semi-heteroskedasticity, the variance differs across locations but remains constant over time; and (iii) under full heteroskedasticity, the variance varies across both dimensions. These cases, summarized in Table 1, are reflected in the diagonal of $\boldsymbol{\Omega}_t$, while the off-diagonal elements are set to zero, implying no cross-correlation either across time or space. Selecting the appropriate variance structure is therefore crucial for obtaining consistent parameter estimates and valid inference in the GSTAR framework.

Table 1. Dimensions Residual Covariance Matrix Structures Based on Location

Homoskedastic	Semi-Heteroskedastic
$\begin{bmatrix} \begin{matrix} \sigma_1^2 & 0 & \cdots & 0 \\ 0 & \sigma_1^2 & \cdots & 0 \\ \vdots & \vdots & \ddots & \vdots \\ 0 & 0 & \cdots & \sigma_1^2 \end{matrix} & \begin{matrix} 0 & 0 & \cdots & 0 \\ 0 & 0 & \cdots & 0 \\ \vdots & \vdots & \ddots & \vdots \\ 0 & 0 & \cdots & 0 \end{matrix} \\ \begin{matrix} 0 & 0 & \cdots & 0 \\ 0 & 0 & \cdots & 0 \\ \vdots & \vdots & \ddots & \vdots \\ 0 & 0 & \cdots & 0 \end{matrix} & \begin{matrix} \sigma_2^2 & 0 & \cdots & 0 \\ 0 & \sigma_2^2 & \cdots & 0 \\ \vdots & \vdots & \ddots & \vdots \\ 0 & 0 & \cdots & \sigma_2^2 \end{matrix} \end{bmatrix}$	$\begin{bmatrix} \begin{matrix} \sigma_1^2 & 0 & \cdots & 0 \\ 0 & \sigma_1^2 & \cdots & 0 \\ \vdots & \vdots & \ddots & \vdots \\ 0 & 0 & \cdots & \sigma_1^2 \end{matrix} & \begin{matrix} 0 & 0 & \cdots & 0 \\ 0 & 0 & \cdots & 0 \\ \vdots & \vdots & \ddots & \vdots \\ 0 & 0 & \cdots & 0 \end{matrix} \\ \begin{matrix} 0 & 0 & \cdots & 0 \\ 0 & 0 & \cdots & 0 \\ \vdots & \vdots & \ddots & \vdots \\ 0 & 0 & \cdots & 0 \end{matrix} & \begin{matrix} \sigma_{2,p+1}^2 & 0 & \cdots & 0 \\ 0 & \sigma_{2,p+2}^2 & \cdots & 0 \\ \vdots & \vdots & \ddots & \vdots \\ 0 & 0 & \cdots & \sigma_{2,T}^2 \end{matrix} \end{bmatrix}$

Heteroskedastic
$\begin{bmatrix} \begin{matrix} \sigma_{1,p+1}^2 & 0 & \cdots & 0 \\ 0 & \sigma_{1,p+1}^2 & \cdots & 0 \\ \vdots & \vdots & \ddots & \vdots \\ 0 & 0 & \cdots & \sigma_{1,p+1}^2 \end{matrix} & \begin{matrix} 0 & 0 & \cdots & 0 \\ 0 & 0 & \cdots & 0 \\ \vdots & \vdots & \ddots & \vdots \\ 0 & 0 & \cdots & 0 \end{matrix} \\ \begin{matrix} 0 & 0 & \cdots & 0 \\ 0 & 0 & \cdots & 0 \\ \vdots & \vdots & \ddots & \vdots \\ 0 & 0 & \cdots & 0 \end{matrix} & \begin{matrix} \sigma_{2,p+1}^2 & 0 & \cdots & 0 \\ 0 & \sigma_{2,p+2}^2 & \cdots & 0 \\ \vdots & \vdots & \ddots & \vdots \\ 0 & 0 & \cdots & \sigma_{2,T}^2 \end{matrix} \end{bmatrix}$

3. RESULTS AND DISCUSSION

3.1 Data Visualization and Preliminary Analysis

Understanding the characteristics of the dataset is a crucial first step before developing an appropriate spatio-temporal model. Therefore, this section outlines the data source, observation sites, temporal coverage, and data partitioning applied for model construction and validation. To capture the rainfall characteristics of the study area, the analysis begins with data visualization and an initial exploratory assessment. The dataset consists of monthly average rainfall in Tasikmalaya Regency, West Java, obtained from NASA POWER (https://power.larc.nasa.gov/data-access-viewer/, accessed on August 15, 2024). Observations were conducted at two sites, Mount Satria (location 1) and Cacaban Salopa (location 2), with their geographic coordinates provided in Table 2 and Fig. 2. The data span the period from January 2000 to December 2023, comprising a total of 288 monthly observations. Approximately 91.67% of the data (264 observations), corresponding to January 2000 - December 2021, were used as training data to construct the short-term forecasting model, while the remaining 8.33% (24 observations), covering January 2022–December 2023, were used as testing data to evaluate model performance.

Table 2. Geographical Coordinates of Observation Sites

No.	Observation Site	Geographical Coordinates	
		Latitude	Longitude
1.	Mount Satria	−7.249	108.008
2.	Cacaban Salopa	−7.514	108.279

Data source: NASA POWER

As summarized in Table 2, the two observation sites are located in different sub-regions of Tasikmalaya Regency, with Mount Satria situated in the western area and Cacaban Salopa in the eastern area. This spatial separation allows the analysis to capture differences in rainfall patterns across locations. To provide a clearer geographical perspective, their positions are illustrated in Fig. 2.

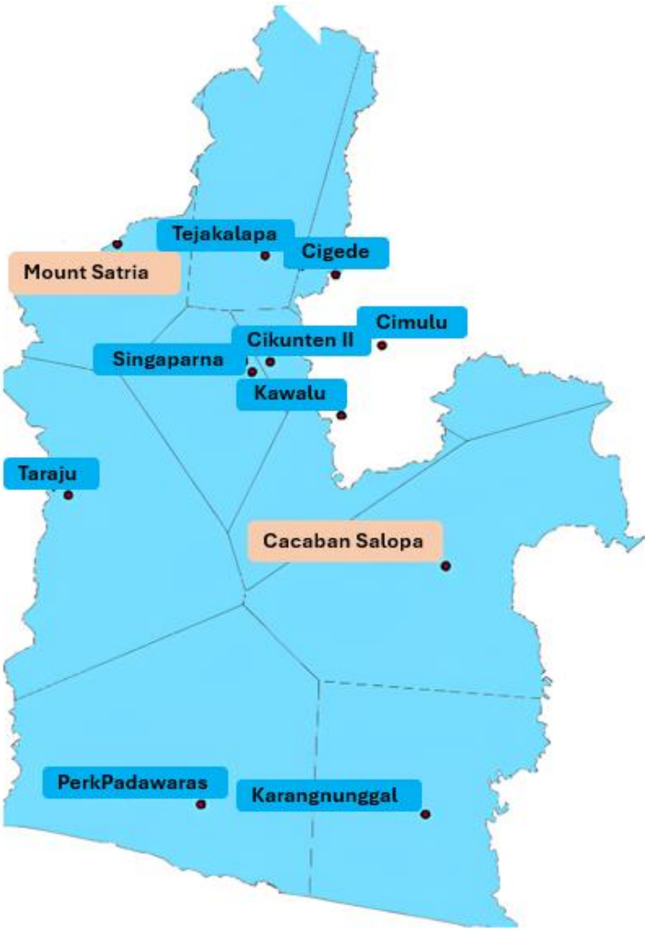

Figure 2. Map of the Selected Rainfall Observation Sites in Tasikmalaya Regency (Map source: Geospatial Information Agency (BIG), Indonesia)

Fig. 2 presents the map of Tasikmalaya Regency highlighting the locations of Mount Satria and Cacaban Salopa. This visualization helps contextualize the spatial distribution of the study sites and provides an overview of their relative positions within the regency.

Subsequently, Fig. 3 illustrates the dynamics of the monthly average rainfall at Mount Satria and Cacaban Salopa over 288 observation periods. The displayed patterns indicate that both locations experience considerable rainfall fluctuations, albeit with distinct characteristics. Mount Satria exhibits relatively uniform fluctuations over time with a generally stable intensity. In contrast, Cacaban Salopa demonstrates an upward trend in rainfall accompanied by several extreme spikes, particularly after the 200th observation. The rainfall peak at Cacaban Salopa exceeds 30 mm, whereas Mount Satria reaches only around 25 mm. These differences highlight that, despite being located within the same region, the rainfall dynamics of the two sites are not entirely homogeneous.

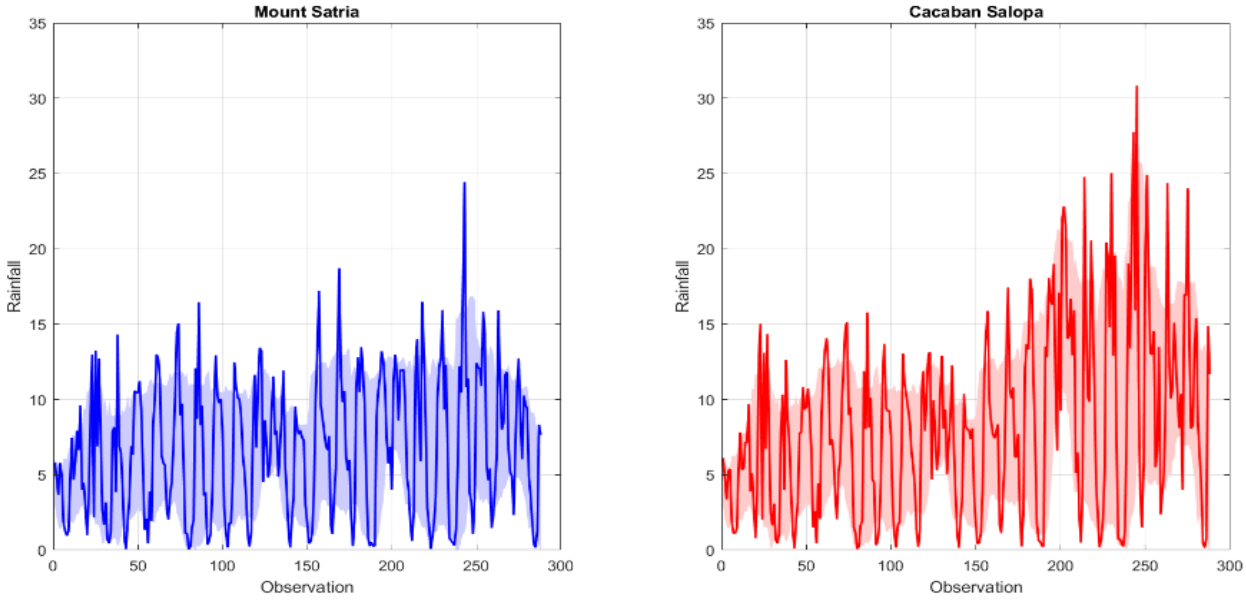

Figure 3. Plots of Monthly Average Rainfall
(Application source: Plots were generated using MATLAB R2024b software)

These visual differences are further supported by the summary statistics presented in Table 3. The mean rainfall at Cacaban Salopa is higher and exhibits greater variability compared to Mount Satria. Similarly, the variance and standard deviation indicate that rainfall at Cacaban Salopa experiences more pronounced fluctuations. Skewness and kurtosis also provide important insights regarding the distribution of rainfall values. The positive skewness observed at both sites indicates that most of the data fall within the low-to-moderate range, while a smaller proportion represents rainfall values considerably higher than the mean. This pattern reflects a right-skewed distribution, where higher values occur more frequently but are not dominant. Furthermore, the higher kurtosis at Cacaban Salopa suggests the presence of more extreme events relative to a normal distribution. These findings are corroborated by the results of the Kolmogorov–Smirnov (KS) test, which indicates that the data at Cacaban Salopa deviate from normality at the 5% significance level. In contrast, both datasets are confirmed to be stationary based on the results of the Augmented Dickey–Fuller (ADF) test.

Table 3. Summary Statistics of Monthly Rainfall

Statistic	Mount Satria	Cacaban Salopa
Observation	288	288
Mean	6.763	8.318
Variance	20.913	37.450
Std. Dev.	4.573	6.119
Skewness	0.391	0.758
Kurtosis	2.645	3.362
KS (P-value)	0.077 (0.063)	0.089 (0.019)
ADF (P-value)	−3.846 (0.001)	−3.747 (0.001)

The spatial relationship between the two sites is clearly evident from the scatter plot and correlation analysis shown in Fig. 4. The correlation coefficient between Mount Satria and Cacaban Salopa is 0.9012 and statistically significant at the 1% level, indicating a very strong and positive association. This implies that the rainfall patterns at both locations tend to move in the same direction. When high rainfall occurs at Mount Satria, a similar event is likely to occur at Cacaban Salopa. This pattern is further reinforced by the data points in the scatter plot, which are concentrated along the diagonal line, reflecting co-movement between the two sites. These findings provide a critical basis for employing spatial models, particularly GSTAR, as rainfall at one location cannot be fully separated from rainfall at the other.

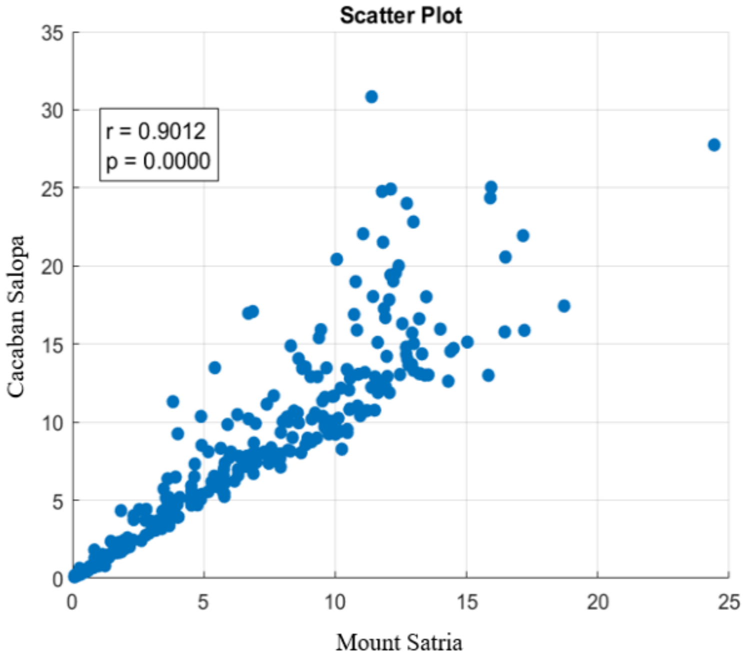

Figure 4. Scatter and correlation plots of rainfall between the two observation sites (Application source: Plots were generated using MATLAB R2024b software)

3.2 GSTAR Modeling

In this study, spatial dependence is represented through a spatial weight matrix. Since the data consist of only two rainfall observation sites, each location has exactly one neighboring site. Under this configuration, any positive weighting scheme such as uniform weights, inverse distance, or inverse distance squared becomes equivalent after row normalization, because the single off-diagonal element in each row is scaled to one. Consequently, the relative spatial influence is invariant to the specific choice of weighting function in a two-location setting. From an identification perspective, the spatial parameter in the GSTAR model is therefore not sensitive to alternative weighting schemes, as no competition among multiple neighbors exists. For this reason, a binary spatial weight matrix with zeros on the main diagonal and ones on the off-diagonal elements is adopted to provide a parsimonious and transparent representation of spatial interaction.

It should be noted that this simplification is specific to the two-location structure of the present study. For datasets involving a larger number of spatial units, geographically informed weighting schemes such as inverse distance or contiguity-based matrices may yield substantively different spatial dynamics. The spatial weight matrix used in this study is presented in Eq. (14)

$$\mathbf{W}^{(1)} = \begin{bmatrix} 0 & 1 \\ 1 & 0 \end{bmatrix}. \tag{14}$$

Once the spatial weight matrix is determined, the model identification process is carried out by analyzing the Space-Time Autocorrelation Function (STACF) and the Space–Time Partial Autocorrelation Function (STPACF) plots. The identification of the GSTAR(p; $\lambda_1, \lambda_2, \dots, \lambda_p$) model can be performed by observing the STACF pattern, which typically exhibits either an exponential decay toward zero or a damped sinusoidal oscillation, as well as the STPACF pattern, which displays a cut-off after the p-th temporal lag and the λ_p-th spatial lag. Fig. 5 presents the STACF and STPACF plots used as the basis for the model identification process.

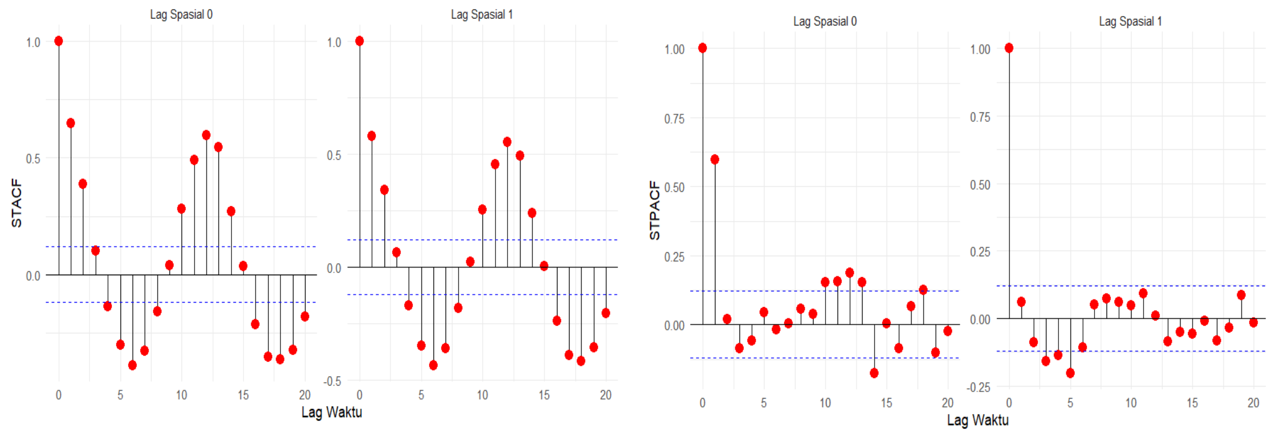

(a) (b)

Figure 5. Plots of STACF and STPACF for Spatial Lags 0 and 1
(a) STACF, (b) STPACF
(Application source: Plots were generated using R software version 4.3.1)

Based on Fig. 5 the STACF analysis for spatial lags 0 and 1, a consistent periodic oscillation pattern is observed, indicating the presence of cyclic or seasonal behavior in the data. Meanwhile, the STPACF plot exhibits a clear cut-off after the first lag for spatial lag 0. For spatial lag 1, the partial correlations drop sharply and become insignificant after the initial lag, suggesting that the spatial influence is limited to the nearest neighboring locations. Based on these findings, the GSTAR model with temporal order $p = 1$ and spatial lag $\lambda = 1$, namely GSTAR(1;1), is considered the most appropriate model structure. Subsequently, parameter estimation for the GSTAR(1;1) model begins with Ordinary Least Squares (OLS) to obtain initial mean parameter estimates by minimizing the sum of squared residuals. The variance parameters of the GARCH components are then estimated using conditional maximum likelihood estimation via an iterative numerical optimization procedure. The estimation follows an alternating framework in which the conditional covariance matrices obtained from the GARCH step are incorporated into a feasible generalized least squares (FGLS) re-estimation of the mean parameters. The procedure is repeated iteratively until convergence, which is assessed based on a predefined tolerance for successive changes in both the mean and variance parameter estimates. The final parameter estimates are presented in Table 4.

In the rainfall analysis for Mount Satria and Cacaban Salopa, three GSTAR(1;1) model specifications were considered. The baseline assumes homoskedastic innovations with constant conditional variance. Diagnostic checks revealed distinct variance behaviors between the two locations: residuals at Mount Satria show no heteroskedasticity, whereas those at Cacaban Salopa exhibit conditional heteroskedasticity. Consequently, ARCH(1) and GARCH(1,1) processes were considered for modeling the conditional variance at Cacaban Salopa, while Mount Satria retains a constant variance. The selection between ARCH(1) and GARCH(1,1) was based on the Akaike Information Criterion (AIC) and Bayesian Information Criterion (BIC), with GARCH(1,1) providing the best balance between model fit and parsimony. Higher-order GARCH models were not considered to maintain consistency with the GSTAR(1,1) mean structure and to avoid unnecessary model complexity given the sample size.

$$\varepsilon_{i,t} = \sqrt{h_{i,t}}\eta_{i,t}, \ \eta_{i,t} \sim N(0,1), \tag{15}$$

where $h_{1,t} = \sigma^2$ follows the homoskedastic component for Mount Satria and $h_{2,t}$ follows ARCH/GARCH dynamics for Cacaban Salopa. In this context, the term "semi-heteroskedastic" is used descriptively to indicate that only Cacaban Salopa exhibits conditional heteroskedasticity. The semi-heteroskedastic framework is employed to allow heterogeneous volatility behavior across locations while maintaining a joint spatial-temporal structure in the conditional mean. Although conditional heteroskedasticity is only detected at Cacaban Salopa, the GSTAR formulation remains necessary to capture cross-location dependence that would be ignored under separate univariate models. An evaluation relative to independent univariate time series modeling indicates that local rainfall dynamics can indeed be represented individually. However, the spatial framework provides a more coherent representation of joint rainfall dynamics by explicitly accounting for cross-location dependence between the two sites. Based on these specifications, the parameter estimates for the three scenarios are summarized below.

Table 4. Parameter Estimation Results and Diagnostic Test Statistics

Model	Variance Assumption	Parameter Estimates		Location	Diagnostics Tests		
		Parameter	Estimate		ARCH Test	K-S Test	L-B Test
GSTAR(1;1)	Homoskedastic	$\phi_{10}^{(1)}$	0.563	Mount Satria	0.078	0.122	< 0.000
		$\phi_{11}^{(1)}$	0.079				
		$\phi_{10}^{(2)}$	0.600	Cacaban Salopa	0.005	0.001	0.220
		$\phi_{11}^{(2)}$	0.053				
GSTAR(1;1)-ARCH(1)	Semi-Heteroscedastic	$\phi_{10}^{(1)}$	0.563	Mount Satria	0.078	0.122	< 0.000
		$\phi_{11}^{(1)}$	0.079				
		$\phi_{10}^{(2)}$	0.662	Cacaban Salopa	0.011	0.003	0.355
		$\phi_{11}^{(2)}$	-0.012				
GSTAR(1;1)-GARCH(1,1)	Semi-Heteroskedastic	$\phi_{10}^{(1)}$	0.563	Mount Satria	0.078	0.122	< 0.000
		$\phi_{11}^{(1)}$	0.079				
		$\phi_{10}^{(2)}$	0.707	Cacaban Salopa	0.872	0.031	0.172
		$\phi_{11}^{(2)}$	-0.059				

Based on the parameter estimation results presented in Table 4, the explicit form of each model can be expressed as follows.

GSTAR(1;1) Model (Homoskedastic)

$$\begin{aligned} Y_{1,t} &= 0.563Y_{1,t-1} + 0.079Y_{2,t-1} + \varepsilon_{1,t}, \qquad & h_{1,t} &= \sigma^2, \\ Y_{2,t} &= 0.600Y_{2,t-1} + 0.053Y_{1,t-1} + \varepsilon_{2,t}, \qquad & h_{2,t} &= \sigma^2. \end{aligned} \tag{16}$$

GSTAR(1;1)-ARCH(1) Model (Semi-Heteroskedastic)

$$\begin{aligned} Y_{1,t} &= 0.563Y_{1,t-1} + 0.079Y_{2,t-1} + \varepsilon_{1,t}, \qquad & h_{1,t} &= \sigma^2, \\ Y_{2,t} &= 0.662Y_{2,t-1} - 0.012Y_{1,t-1} + \varepsilon_{2,t}, \qquad & h_{2,t} &= 20.083 + 0.092\varepsilon_{2,t-1}^2. \end{aligned} \tag{17}$$

GSTAR(1;1)-GARCH(1,1) Model (Semi-Heteroskedastic)

$$\begin{aligned} Y_{1,t} &= 0.563Y_{1,t-1} + 0.079Y_{2,t-1} + \varepsilon_{1,t}, \qquad & h_{1,t} &= \sigma^2, \\ Y_{2,t} &= 0.707Y_{2,t-1} - 0.059Y_{1,t-1} + \varepsilon_{2,t}, \qquad & h_{2,t} &= 0.159 + 0.066\varepsilon_{2,t-1}^2 + 0.933h_{2,t-1}. \end{aligned} \tag{18}$$

Analysis of Table 4 together with Eqs. (15)-(17) highlights distinct dynamics across locations. At Mount Satria, parameter estimates remain stable under all specifications, reflecting a relatively consistent rainfall pattern that is primarily influenced by local persistence. Diagnostic checks confirm the absence of strong heteroskedasticity, and the residuals approximate normality, though minor autocorrelation persists. As a result, augmenting the model with ARCH(1) or GARCH(1,1) effects does not yield substantial changes or improvements at this site. By contrast, rainfall at Cacaban Salopa exhibits greater variability. When conditional heteroskedasticity is explicitly modeled, the local rainfall coefficient increases, while the cross-location effect changes sign from positive to negative. This shift may reflect underlying climatic or geographic mechanisms, such as orographic influences or prevailing wind patterns. Moreover, diagnostic tests indicate that the standard GSTAR(1;1) specification fails to capture the volatility structure, whereas ARCH(1) and GARCH(1,1) terms stabilize conditional variance and reduce residual autocorrelation. In the GARCH(1,1) case, the persistence parameter satisfies the stationarity condition ($\alpha + \beta < 1$) but is very close to unity, indicating highly persistent volatility.

Despite the diagnostic improvements shown in Table 4, predictive accuracy remains constrained. As presented in Table 5, the testing error metrics (MSE, MAE, RMSE) for GSTAR(1;1)-ARCH(1) and GSTAR(1;1)-GARCH(1,1) exceed those of the baseline GSTAR(1;1), particularly at Cacaban Salopa, where testing RMSE increases by approximately 60%. This apparent discrepancy reflects the fundamental distinction between modeling conditional variance and optimizing point forecasts. ARCH and GARCH components improve residual properties by stabilizing time-varying variance; however, forecast accuracy measures such as MSE and RMSE evaluate mean prediction performance, which is governed solely by the conditional mean equation. At Cacaban Salopa, the estimated GARCH(1,1) parameters indicate highly persistent volatility ($\alpha + \beta$ close to unity), suggesting near-integrated behavior. Such persistence may increase parameter uncertainty and reduce adaptability in short out-of-sample periods, thereby weakening generalization performance. In contrast, rainfall variability at Mount Satria is relatively stable, and conditional variance remains nearly constant, resulting in minimal differences in forecasting performance across specifications. Therefore, improved heteroskedasticity diagnostics do not necessarily translate into superior predictive accuracy, especially in finite samples with limited testing observations.

Table 5. Training and Testing Performance Metrics of GSTAR-Based Models

Location	Model	Training			Testing		
		MSE	MAE	RMSE	MSE	MAE	RMSE
Mount Satria	GSTAR(1;1)	12.179	2.730	3.490	7.684	2.485	2.772
	GSTAR(1;1)-ARCH(1)	12.184	2.727	3.491	7.613	2.461	2.759
	GSTAR(1;1)-GARCH(1,1)	12.179	2.730	3.490	7.684	2.485	2.772
Cacaban Salopa	GSTAR(1;1)	22.071	3.542	4.698	22.758	3.944	3.214
	GSTAR(1;1)-ARCH(1)	22.134	3.543	4.705	26.356	4.017	5.134
	GSTAR(1;1)-GARCH(1,1)	22.155	3.537	4.708	26.426	4.019	5.141

Based on the diagnostic results presented in Table 4, the GSTAR(1;1)-GARCH(1,1) model effectively reduces heteroskedasticity, as indicated by ARCH test significance values that mostly exceed 0.05. However, the assumption of residual normality is not fully satisfied, as reflected in the Kolmogorov-Smirnov (K-S) test results, and autocorrelation remains an issue at Mount Satria according to the Ljung-Box (L-B) test. Although the residual normality assumption is violated, this does not invalidate the parameter estimation. Under the quasi-maximum likelihood framework, GARCH estimators remain consistent and asymptotically normal even when innovations deviate from Gaussianity, provided finite second moments exist. Nevertheless, non-normality may reduce estimation efficiency and affect inference accuracy, particularly in the presence of heavy-tailed behavior. Given that rainfall data are typically skewed and leptokurtic, such deviations from normality are not unexpected. The presence of residual autocorrelation at Mount Satria suggests that some temporal dependence may remain unexplained by the GSTAR(1,1) specification. Higher-order GSTAR models or seasonal components could potentially capture this remaining dependence; however, they were not explored in this study to maintain model parsimony and to focus on the proposed semi-heteroskedastic framework. These findings indicate that, although GSTAR(1;1)-GARCH(1,1) is effective in modeling conditional heteroskedasticity, limitations remain in capturing the full distributional characteristics of rainfall residuals. Alternative specifications, such as GARCH models with Student's t or skewed innovation distributions, as well as non-parametric approaches, may provide more robust representations and are suggested for future research. Therefore, the forecasting results should be interpreted with caution and are presented primarily to illustrate model behavior rather than for direct decision-making.

Figs. 6 and 7 presents the rainfall prediction results for the two study locations, Mount Satria and Cacaban Salopa. The graphs in the upper row depict the predictions during the training period, where the black solid line represents the observed data, and the red dashed line indicates the model's predicted values. The graphs in the lower row show the predictions during the testing period, with the black solid line representing the observed data and the orange dashed line representing the model predictions.

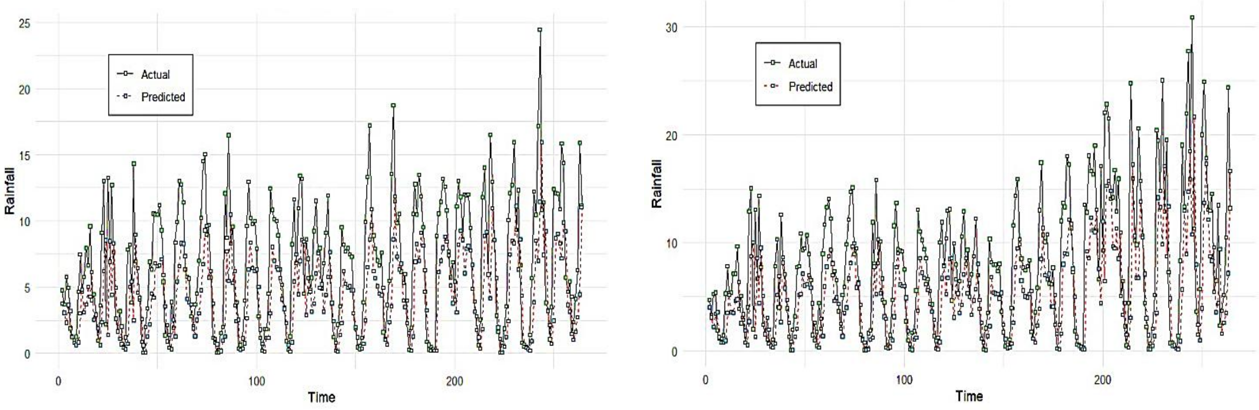

(a) (b)

Figure 6. Actual and Predicted Rainfall Plots for the Training Period
(a) Mount Satria, (b) Cacaban Salopa
(Application source: Plots were generated using R software version 4.3.1)

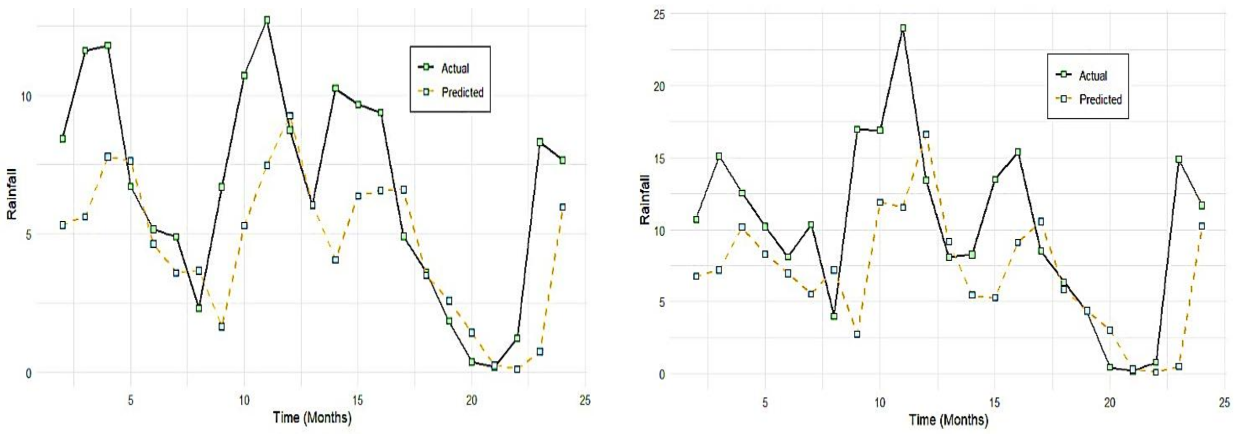

(a) (b)

Figure 7. Actual and Predicted Rainfall Plots for the Testing Period
(a) Mount Satria, (b) Cacaban Salopa
(Application source: Plots were generated using R software version 4.3.1)

Based on Fig. 7, the five-step-ahead forecasts produced by the GSTAR(1,1)-GARCH(1,1) model exhibit similar declining trend patterns at both Mount Satria and Cacaban Salopa, which are consistent with the observed seasonal behavior of rainfall. These forecasts are presented to illustrate the dynamic behavior of the proposed GSTAR-GARCH framework rather than to provide comprehensive practical validation. No benchmarking against naive forecasts, climatological means, or alternative spatio-temporal methods was conducted, and model evaluation was limited to absolute error measures (MSE, MAE, and RMSE). Consequently, the practical forecasting performance should be interpreted with caution, and more extensive comparative validation using relative accuracy metrics is left for future research.

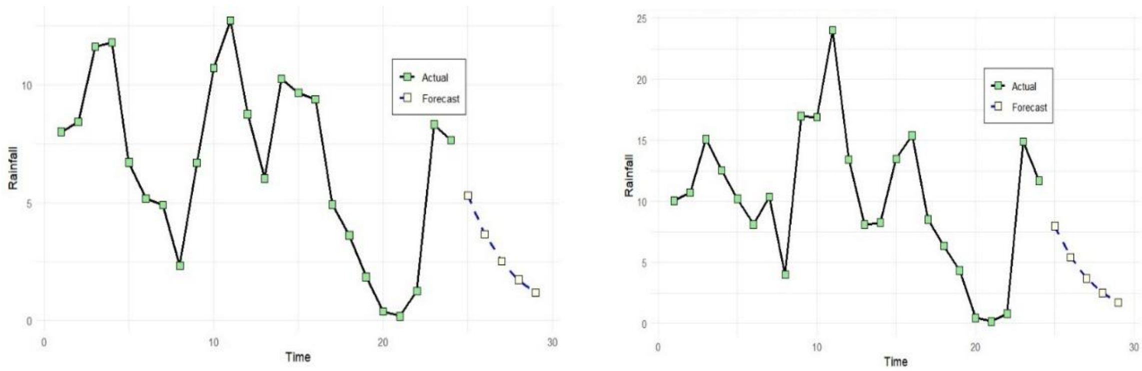

(a) (b)

Figure 8. Actual and Forecasted Rainfall Using the GSTAR-GARCH Approach for the Testing Period
(a) Mount Satria, (b) Cacaban Salopa
(Application source: Plots were generated using R software version 4.3.1)

The five-step-ahead forecasts produced by the GSTAR(1;1)-GARCH(1,1) model show a gradual decline in rainfall at both study sites, Mount Satria and Cacaban Salopa. The decrease is steady and matches climatological expectations. The observed data end in December 2023 during the rainy season while the forecast period covers January to May 2024, marking the transition from the rainy to the dry season. The model's forecasted downward trend aligns with the typical seasonal dynamics of tropical regions like Indonesia. No anomalies such as constant or extreme values are observed and the forecast curves maintain the natural variability seen in the historical data. Overall, these results indicate that the model effectively captures both the spatio-temporal patterns and the inherent dynamics of rainfall at the study sites.

The results of this study confirm that rainfall dynamics differ substantially across the two locations. At Mount Satria, residual variance is relatively stable, making the basic GSTAR(1;1) specification adequate. In contrast, Cacaban Salopa exhibits pronounced volatility, violating the homoskedasticity assumption. Incorporating the GARCH(1,1) component effectively mitigates conditional heteroskedasticity, as indicated by the ARCH-LM test results. Thus, the primary contribution of the GSTAR(1;1)-GARCH(1,1) model lies in improving variance specification and inferential adequacy rather than enhancing short-term point forecasting accuracy. Although diagnostic properties improve, testing performance at Cacaban Salopa deteriorates. This outcome is consistent with the theoretical distinction between modeling conditional variance and optimizing conditional mean forecasts. The highly persistent volatility ($\alpha + \beta$ close to unity) suggests near-integrated behavior, which may increase parameter uncertainty and reduce adaptability in a short out-of-sample window. Therefore, improved residual diagnostics do not necessarily translate into superior predictive performance, particularly in finite samples.

Compared to previous research integrating GSTAR(1;1) with ARCH(1) [12], [14], [24], [25], [26], [27], [28], this study extends the framework by allowing persistent volatility through GARCH(1,1). While this enhances volatility representation and inferential accuracy, predictive performance for the testing data at Cacaban Salopa remains constrained. From an application perspective, five-step-ahead forecasts indicate a declining rainfall trend, consistent with seasonal patterns in tropical regions, though residual assumptions are not fully satisfied. Consequently, forecasts should be interpreted as illustrative rather than prescriptive. The main limitation lies in residuals' deviation from normality, which restricts the model's capacity to capture extreme rainfall variations. Future research should explore more flexible heteroskedastic models, such as GJR-GARCH, and incorporate non-normal residual distributions to yield more adaptive models and reliable rainfall forecasts in regions with high weather variability.

The main limitation of this study lies in the residuals' deviation from normality, which restricts the model's capacity to capture extreme rainfall variations. Prediction accuracy is also lower at locations with highly fluctuating rainfall, reflecting the model's sensitivity to spatio-temporal volatility. Although GSTAR(1;1)-GARCH(1,1) effectively mitigates heteroskedasticity and models spatio-temporal dependencies, it still struggles with extreme events and non-normal residual distributions. Future research should explore more flexible heteroskedastic models, such as GJR-GARCH, and incorporate non-normal residual distributions. Such approaches are expected to yield more adaptive models and more reliable rainfall forecasts, particularly in regions characterized by high weather variability.

4. CONCLUSION

This study proposes a spatio-temporal rainfall modeling framework that integrates GSTAR dynamics with conditional heteroskedastic volatility through a GSTAR(1;1)-GARCH(1,1) specification. The model captures both cross-location dependence in the mean structure and time-varying variance behavior across spatial units. The main novelty of this work lies in extending GSTAR modeling by incorporating a semi-heteroskedastic GARCH(1,1) process, allowing persistent spatial-temporal volatility to be represented—a feature not systematically addressed in previous studies. Empirical results demonstrate that adding the GARCH component improves residual diagnostics, particularly at Cacaban Salopa, where rainfall exhibits highly variable patterns. Despite these improvements in variance modeling, residuals remain non-normal, and out-of-sample prediction errors increase relative to the baseline GSTAR(1;1), illustrating the well-known forecasting paradox: improving variance representation enhances inferential adequacy but does not guarantee superior point forecast accuracy. The highly persistent volatility ($\alpha + \beta$ close to unity) further limits short-term predictive adaptability, especially in finite testing samples.

The analysis employs a simple binary spatial weight matrix due to the two-location dataset. While this choice provides a parsimonious and transparent representation of spatial interactions, more complex spatial weighting schemes would be required to capture richer spatial dependence in larger networks. Five-step-ahead forecasts reveal a declining rainfall tendency consistent with seasonal transition from the rainy to the dry period, confirming that the model reproduces observed temporal dynamics, albeit without fully satisfying residual normality assumptions. The main limitations of this study lie in residual non-normality and the limited spatial scope, which constrain the model's ability to capture extreme events and complex cross-location variance interactions. Future research should explore more flexible heteroskedastic models, such as GJR-GARCH, incorporate non-normal innovation structures, and evaluate higher-dimensional spatial configurations to improve robustness and potential gains in predictive performance. Overall, the GSTAR(1;1)-GARCH(1,1) framework provides a valuable tool for understanding rainfall uncertainty and volatility, even if short-term predictive accuracy remains constrained.

Author Contributions

Nurhayati: Conceptualization, Methodology, Visualization, Writing-Original Draft, Validation, Software. Muhammad Rozzaq Hamidi: Software, Validation, Investigation, Resources, Data Curation, Review. Utriweni Mukhaiyar: Conceptualization, Methodology, Supervision, Formal Analysis, Writing-Review and Editing, validation. Kurnia Novita Sari: Supervision, Validation, Writing-Review and Editing. All authors discussed the results and contributed to the final manuscript.

Funding Statement

This research was funded by the Ministry of Higher Education, Science, and Technology (Kementerian Pendidikan Tinggi, Sains, dan Teknologi, Kemdiktisaintek) of Indonesia through the PDD 2025 grant, under Contract No. 015/C3/DT.05.00/PL/2025.

Acknowledgment

The authors would like to thank the anonymous reviewers for their insightful comments and valuable suggestions that significantly improved this article. The authors also acknowledge the NASA POWER Project for providing the rainfall dataset used in this study.

Declarations

The authors state that there are no conflicts of interest concerning the publication of this study. All results and interpretations in this paper are exclusively the responsibility of the authors.

Declaration of Generative AI and AI-assisted technologies

The authors declare that no generative AI or AI-assisted technologies were used in the preparation of this manuscript, including for writing, editing, data analysis, or the creation of tables and figures.

REFERENCES

[1] Y. Yundari, N. M. Huda, U. Pasaribu, and U. Mukhaiyar, "STATIONARY PROCESS IN GSTAR(1;1) THROUGH KERNEL FUNCTION APPROACH," *AIP Conf. Proc.*, vol. 2268, no. 1, 2020. doi: https://doi.org/10.1063/5.0016808.

[2] F. Hestuningtias and M. H. S. Kurniawan, "THE IMPLEMENTATION OF THE GENERALIZED SPACE-TIME AUTOREGRESSIVE (GSTAR) MODEL FOR INFLATION PREDICTION," *Enthusiastic Int. J. Appl. Stat. Data Sci.*, vol. 3, no. 2, pp. 176–188, 2023. doi: https://doi.org/10.20885/enthusiastic.vol3.iss2.art5.

[3] L. Zhao, S. Sen Gupta, A. Khan, and R. Luo, *Temporal analysis of the entire ethereum blockchain network*, vol. 1, no. 1. Association for Computing Machinery, 2021. doi: https://doi.org/10.1145/3442381.3449916.

[4] I. Franch-Pardo, B. M. Napoletano, F. Rosete-Verges, and L. Billa, "SPATIAL ANALYSIS AND GIS IN THE STUDY OF COVID-19. A REVIEW," *Sci. Total Environ.*, vol. 739, p. 140033, 2020. doi: https://doi.org/10.1016/j.scitotenv.2020.140033.

[5] S. Suhartono, D. D. Prastyo, H. Kuswanto, and M. H. Lee, "COMPARISON BETWEEN VAR, GSTAR, FFNN-VAR AND FFNN-GSTAR MODELS FOR FORECASTING OIL PRODUCTION," *Matematika*, vol. 34, no. 1, pp. 103–111, 2018. doi: https://doi.org/10.11113/matematika.v34.n1.1040.

[6] X. Lu, M. Salehi, M. Haenggi, E. Hossain, and H. Jiang, "STOCHASTIC GEOMETRY ANALYSIS OF SPATIAL-TEMPORAL PERFORMANCE IN WIRELESS NETWORKS: A TUTORIAL," *IEEE Commun. Surv. Tutorials*, vol. 23, no. 4, pp. 2753–2801, 2021. doi: https://doi.org/10.1109/COMST.2021.3104581.

[7] P. Zhu, J. Li, and Y. Hou, "APPLYING A POPULATION FLOW–BASED SPATIAL WEIGHT MATRIX IN SPATIAL ECONOMETRIC MODELS: CONCEPTUAL FRAMEWORK AND APPLICATION TO COVID-19 TRANSMISSION ANALYSIS," *Ann. Am. Assoc. Geogr.*, vol. 112, no. 8, pp. 2266–2286, 2022. doi: https://doi.org/10.1080/24694452.2022.2060791.

[8] C. Lam and P. C. L. Souza, "ESTIMATION AND SELECTION OF SPATIAL WEIGHT MATRIX IN A SPATIAL LAG MODEL," *J. Bus. Econ. Stat.*, vol. 38, no. 3, pp. 693–710, 2020. doi: https://doi.org/10.1080/07350015.2019.1569526.

[9] U. Mukhaiyar *et al.*, "THE GENERALIZED STAR MODELLING WITH THREE-DIMENSIONAL OF SPATIAL WEIGHT MATRIX IN PREDICTING THE INDONESIA PEATLAND'S WATER LEVEL," *Environ. Sci. Eur.*, vol. 36, no. 1, 2024. doi: https://doi.org/10.1186/s12302-024-00979-6.

[10] R. Utami, U. Mukhaiyar, N. Mardiyah, Y. Sa'adah, and E. Widyawati, "SPATIAL WEIGHTING SELECTION IN GSTAR AND S-GSTAR MODELS FOR TEMPERATURE PREDICTION," *J. Mat. Stat. dan Komputasi*, vol. 20, no. 3, pp. 639–653, 2024. doi: https://doi.org/10.20956/j.v20i3.34305.

[11] S. Borovkova, H. P. Lopuhaä, and B. N. Ruchjana, "CONSISTENCY AND ASYMPTOTIC NORMALITY OF LEAST SQUARES ESTIMATORS IN GENERALIZED STAR MODELS," *Stat. Neerl.*, vol. 62, no. 4, pp. 482–508, 2008. doi: https://doi.org/10.1111/j.1467-9574.2008.00391.x.

[12] U. Mukhaiyar and S. Ramadhani, "THE GENERALIZED STAR MODELING WITH HETEROSCEDASTIC EFFECTS,"

CAUCHY J. Mat. Murni dan Apl., vol. 7, no. 2, pp. 158–172, 2022. doi: https://doi.org/10.18860/ca.v7i2.13097.

[13] N. Nurhayati, R. Hamidi, M., U. Mukhaiyar, and N. Sari, K., “CROSS-CORRELATION ANALYSIS IN EVALUATING SPATIO-TEMPORAL DATA DEPENDENCE OF CLIMATE VARIABLES THROUGH THE GSTAR MODEL,” *JMSK J. Mat. Stat. dan Komputasi*, vol. 21, no. 3, pp. 813–831, 2025. doi: https://doi.org/10.20956/j.v21i3.43665.

[14] P. Monika, B. N. Ruchjana, and A. S. Abdullah, “GSTARI-X-ARCH MODEL WITH DATA MINING APPROACH FOR FORECASTING CLIMATE IN WEST JAVA,” *Computation*, vol. 10, no. 12, 2022. doi: https://doi.org/10.3390/computation10120204.

[15] M. Sheraz and I. Nasir, “INFORMATION-THEORETIC MEASURES AND MODELING STOCK MARKET VOLATILITY: A COMPARATIVE APPROACH,” *Risks*, vol. 9, no. 5, 2021. doi: https://doi.org/10.3390/risks9050089.

[16] B. Dinga, J. H. Claver, K. K. Cletus, and S. F. Che, “MODELING AND PREDICTING EXCHANGE RATE VOLATILITY: APPLICATION OF SYMMETRIC GARCH AND ASYMMETRIC EGARCH AND GJR-GARCH MODELS,” *J. Cameroon Acad. Sci.*, vol. 19, no. 2, pp. 155–178, 2023 doi:. https://doi.org/10.4314/jcas.v19i2.6.

[17] P. R. Dewick, “ON FINANCIAL DISTRIBUTIONS MODELLING METHODS: APPLICATION ON REGRESSION MODELS FOR TIME SERIES,” *J. Risk Financ. Manag.*, vol. 15, no. 10, p. 461, 2022. doi: https://doi.org/10.3390/jrfm15100461.

[18] C. Spulbar, R. Birau, J. Trivedi, I. T. Hawaldar, and E. L. Minea, “TESTING VOLATILITY SPILLOVERS USING GARCH MODELS IN THE JAPANESE STOCK MARKET DURING COVID-19,” *Invest. Manag. Financ. Innov.*, vol. 19, no. 1, pp. 262–273, 2022. doi: https://doi.org/10.21511/imfi.19(1).2022.20.

[19] M. Zahid, F. Iqbal, and D. Koutmos, “FORECASTING BITCOIN VOLATILITY USING HYBRID GARCH MODELS WITH MACHINE LEARNING,” *Risks*, vol. 10, no. 12, 2022. doi: https://doi.org/10.3390/risks10120237.

[20] R. F. Engle and V. K. Ng, “MEASURING AND TESTING THE IMPACT OF NEWS ON VOLATILITY,” *J. Finance*, vol. 48, no. 5, p. 1749, 1993. doi: https://doi.org/10.2307/2329066.

[21] T. Bollerslev, “GENERALIZED AUTOREGRESSIVE CONDITIONAL HETEROSKEDASTICITY,” *J. Econom.*, vol. 31, no. 3, pp. 307–327, 1986. doi: https://doi.org/10.1016/0304-4076(86)90063-1

[22] D. Rakshit, R. K. Paul, M. Yeasin, W. Emam, Y. Tashkandy, and C. Chesneau, “MODELING ASYMMETRIC VOLATILITY: A NEWS IMPACT CURVE APPROACH,” *Mathematics*, vol. 11, no. 13, pp. 1–14, 2023. doi: https://doi.org/10.3390/math11132793

[23] U. Mukhaiyar, B. I. Bilad, and U. S. Pasaribu, “THE GENERALIZED STAR MODELLING WITH MINIMUM SPANNING TREE APPROACH OF WEIGHT MATRIX FOR COVID-19 CASE IN JAVA ISLAND,” *J. Phys. Conf. Ser.*, vol. 2084, no. 1, 2021. doi: https://doi.org/10.1088/1742-6596/2084/1/012003

[24] H. Bonar, B. N. Ruchjana, and G. Darmawan, “DEVELOPMENT OF GENERALIZED SPACE TIME AUTOREGRESSIVE INTEGRATED WITH ARCH ERROR (GSTARI - ARCH) MODEL BASED ON CONSUMER PRICE INDEX PHENOMENON AT SEVERAL CITIES IN NORTH SUMATERA PROVINCE,” *AIP Conf. Proc.*, vol. 1827, no. March 2017, 2017. doi: https://doi.org/10.1063/1.4979425

[25] S. Borovkova and R. Lopuhaa, “SPATIAL GARCH: A SPATIAL APPROACH TO MULTIVARIATE VOLATILITY MODELING,” *SSRN Electron. J.*, vol. 1, no. 1, pp. 1–33, 2012. doi: https://doi.org/10.2139/ssrn.2176781

[26] N. Nainggolan and J. Titaley, “DEVELOPMENT OF GENERALIZED SPACE TIME AUTOREGRESSIVE (GSTAR) MODEL,” *AIP Conf. Proc.*, vol. 1827, no. March, 2017. doi: https://doi.org/10.1063/1.4979450

[27] P. Monika, B. N. Ruchjana, A. S. Abdullah, and R. Budiarto, “DEVELOPMENT OF GSTARIMA-ARCH MODEL FOR RAINFALL FORECASTING IN JAVA ISLAND USING BIG DATA ANALYTICS,” *Appl. Math. Inf. Sci.*, vol. 19, no. 3, pp. 577–593, 2025. doi: https://doi.org/10.18576/amis/190309

[28] M. Alawiyah, D. A. Kusuma, and B. N. Ruchjana, “GSTARI-ARCH MODEL AND APPLICATION ON POSITIVE CONFIRMED DATA FOR COVID-19 IN WEST JAVA,” *Media Stat.*, vol. 14, no. 2, pp. 146–157, 2022. doi: https://doi.org/10.14710/medstat.14.2.146-157

[29] S. Ling and M. McAleer, “ASYMPTOTIC THEORY FOR A VECTOR ARMA-GARCH MODEL,” *Econom. Theory*, vol. 19, no. 2, pp. 280–310, 2003. doi: https://doi.org/10.1017/S0266466603192092

[30] R. F. Engle, “AUTOREGRESSIVE CONDITIONAL HETEROSCEDASTICITY WITH ESTIMATES OF THE VARIANCE OF UNITED KINGDOM INFLATION,” *Econometrica*, vol. 50, no. 4, pp. 987–1007, 1982. doi: https://doi.org/10.2307/1912773

[31] T. Bollerslev, “THE STORY OF GARCH: A PERSONAL ODYSSEY,” *J. Econom.*, vol. 234, pp. 96–100, 2023. doi: https://doi.org/10.1016/j.jeconom.2023.01.015

[32] A. J. McNeil and R. Frey., *Quantitative Risk Management.* Princeton: NJ: Princeton University Press., 2005.

[33] B. N. Ruchjana, “A GENERALIZED SPACE TIME AUTOREGRESSIVE MODEL AND ITS APPLICATION TO OIL PRODUCTION DATA,” Institut Teknologi bandung, 2002.

[34] U. Mukhaiyar and U. S. Pasaribu, “A NEW PROCEDURE FOR GENERALIZED STAR MODELING USING IACM APPROACH,” *ITB J. Sci.*, vol. 44 A, no. 2, pp. 179–192, 2012. doi: https://doi.org/10.5614/itbj.sci.2012.44.2.7

[35] Yundari, U. S. Pasaribu, U. Mukhaiyar, and M. N. Heriawan, “SPATIAL WEIGHT DETERMINATION OF GSTAR(1;1) MODEL BY USING KERNEL FUNCTION,” *J. Phys. Conf. Ser.*, vol. 1028, no. 1, 2018. doi: https://doi.org/10.1088/1742-6596/1028/1/012223

[36] A. S. Abdullah *et al.*, “IMPLEMENTATION OF GENERALIZED SPACE TIME AUTOREGRESSIVE (GSTAR)-KRIGING MODEL FOR PREDICTING RAINFALL DATA AT UNOBSERVED LOCATIONS IN WEST JAVA,” *Appl. Math. Inf. Sci.*, vol. 12, no. 3, pp. 607–615, 2018. doi: https://doi.org/10.18576/amis/120316

[37] D. Masteriana, M. I. Riani, and U. Mukhaiyar, “GENERALIZED STAR (1;1) MODEL WITH OUTLIER - CASE STUDY OF BEGAL IN MEDAN, NORTH SUMATERA,” *J. Phys. Conf. Ser.*, vol. 1245, no. 1, pp. 0–9, 2019. doi: https://doi.org/10.1088/1742-6596/1245/1/012046

[38] Yundari, U. S. Pasaribu, and U. Mukhaiyar, “ERROR ASSUMPTIONS ON GENERALIZED STAR MODEL,” *J. Math. Fundam. Sci.*, vol. 49, no. 2, pp. 136–155, 2017. doi: https://doi.org/10.5614/j.math.fund.sci.2017.49.2.4

[39] N. M. Huda, U. Mukhaiyar, and N. Imro’ah, “AN ITERATIVE PROCEDURE FOR OUTLIER DETECTION IN GSTAR(1;1) MODEL,” *Barekeng*, vol. 16, no. 3, pp. 975–984, 2022. doi: https://doi.org/10.30598/barekengvol16iss3pp975-984

[40] U. Mukhaiyar, N. M. Huda, K. N. Sari, and U. S. Pasaribu, “ANALYSIS OF GENERALIZED SPACE TIME

AUTOREGRESSIVE WITH EXOGENOUS VARIABLE (GSTARX) MODEL WITH OUTLIER FACTOR," *J. Phys. Conf. Ser.*, vol. 1496, no. 1, 2020. doi: https://doi.org/10.1088/1742-6596/1496/1/012004

[41] N. M. Huda, U. Mukhaiyar, and U. S. Pasaribu, "THE APPROXIMATION OF GSTAR MODEL FOR DISCRETE CASES THROUGH INAR MODEL," *J. Phys. Conf. Ser.*, vol. 1722, no. 1, 2021. doi: https://doi.org/10.1088/1742-6596/1722/1/012100

[42] Y. Yundari and S. W. Rizki, "INVERTIBILITY OF GENERALIZED SPACE-TIME AUTOREGRESSIVE MODEL WITH RANDOM WEIGHT," *CAUCHY J. Mat. Murni dan Apl.*, vol. 6, no. 4, pp. 246–259, 2021. doi: https://doi.org/10.18860/ca.v6i4.11254

[43] H. Pratiwi, N. Imro'ah, and N. M. Huda, "FOREST FIRE ANALYSIS FROM PERSPECTIVE OF SPATIAL- TEMPORAL USING GSTAR MODEL," *BAREKENG J. Math. Its Appl.*, vol. 19, no. 2, pp. 1379–1392, 2025. doi: https://doi.org/10.30598/barekengvol19iss2pp1379-1392

[44] N. M. Huda and N. Imro'ah, "DETERMINATION OF THE BEST WEIGHT MATRIX FOR THE GENERALIZED SPACE TIME AUTOREGRESSIVE (GSTAR) MODEL IN THE COVID-19 CASE ON JAVA ISLAND, INDONESIA," *Spat. Stat.*, vol. 54, 2023. doi: https://doi.org/10.1016/j.spasta.2023.100734

[45] N. Nurhayati, U. S. Pasaribu, and O. Neswan, "APPLICATION OF GENERALIZED SPACE-TIME AUTOREGRESSIVE MODEL ON GDP DATA IN WEST EUROPEAN COUNTRIES," *J. Probab. Stat.*, vol. 2012, 2012. doi: https://doi.org/10.1155/2012/867056

[46] U. Mukhaiyar, "THE GOODNESS OF GENERALIZED STAR IN SPATIAL DEPENDENCY OBSERVATIONS MODELING," *AIP Conf. Proc.*, vol. 1692, pp. 1–5, 2015. doi: https://doi.org/10.1063/1.4936436

[47] R. F. Nugraha, S. Setiyowati, U. Mukhaiyar, and A. Yuliawati, "PREDICTION OF OIL PALM PRODUCTION USING THE WEIGHTED AVERAGE OF FUZZY SETS CONCEPT APPROACH," *AIP Conf. Proc.*, vol. 1692, pp. 1–5, 2015. doi: https://doi.org/10.1063/1.4936440

[48] F. I. N. Fadlilah, U. Mukhaiyar, and F. Fahmi, "THE GENERALIZED STAR(1,1) MODELING WITH TIME CORRELATED ERRORS TO RED-CHILI WEEKLY PRICES OF SOME TRADITIONAL MARKETS IN BANDUNG, WEST JAVA," *AIP Conf. Proc.*, vol. 1692, 2015. doi: https://doi.org/10.1063/1.4936442

[49] U. Mukhaiyar, N. M. Huda, R. R. K. Novita Sari, and U. S. Pasaribu, "MODELING DENGUE FEVER CASES BY USING GSTAR(1;1) MODEL WITH OUTLIER FACTOR," *J. Phys. Conf. Ser.*, vol. 1366, no. 1, 2019. doi: https://doi.org/10.1088/1742-6596/1366/1/012122

[50] U. S. Pasaribu, U. Mukhaiyar, N. M. Huda, K. N. Sari, and S. W. Indratno, "MODELLING COVID-19 GROWTH CASES OF PROVINCES IN JAVA ISLAND BY MODIFIED SPATIAL WEIGHT MATRIX GSTAR THROUGH RAILROAD PASSENGER'S MOBILITY," *Heliyon*, vol. 7, no. 2, p. e06025, 2021. doi: https://doi.org/10.1016/j.heliyon.2021.e06025

[51] J. Hu, S. Wang, and J. Mao, "SHORT TIME PM2.5 PREDICTION MODEL FOR BEIJING-TIANJIN-HEBEI REGION BASED ON GENERALIZED SPACE TIME AUTOREGRESSIVE (GSTAR)," *IOP Conf. Ser. Earth Environ. Sci.*, vol. 358, no. 2, pp. 0–6, 2019. doi: https://doi.org/10.1088/1755-1315/358/2/022075

[52] M. A. ZEWDİE, G. G. WUBİT, and A. W. AYELE, "G-STAR MODEL FOR FORECASTING SPACE-TIME VARIATION OF TEMPERATURE IN NORTHERN ETHIOPIA," *Turkish J. Forecast.*, vol. 02, no. 1, pp. 9–19, 2018. doi: https://doi.org/10.34110/forecasting.437599

[53] H. Pramoedyo, A. Ashari, and A. Fadliana, "APPLICATION OF GSTAR KRIGING MODEL IN FORECASTING AND MAPPING COFFEE BERRY BORER ATTACK IN PROBOLINGGO DISTRICT," *J. Phys. Conf. Ser.*, vol. 1563, no. 1, 2020. doi: https://doi.org/10.1088/1742-6596/1563/1/012005

[54] R. Jonathan, Yundari, Nurhasanah, and O. Y. E. Nada, "APPLICATION OF GSTAR(1,1) MODEL FOR LAYER PEAT SOIL PREDICTED BASED ON RESISTIVITY LOG DATA," *J. Phys. Conf. Ser.*, vol. 2106, no. 1, pp. 0–7, 2021. doi: https://doi.org/10.1088/1742-6596/2106/1/012031

[55] U. S. Pasaribu, U. Mukhaiyar, M. N. Heriawan, and Y. Yundari, "GENERALIZED SPACE-TIME AUTOREGRESSIVE MODELING OF THE VERTICAL DISTRIBUTION OF COPPER AND GOLD GRADES WITH A PORPHYRY-DEPOSIT CASE STUDY," *Int. J. Adv. Sci. Eng. Inf. Technol.*, vol. 12, no. 5, pp. 2030–2038, 2022. doi: https://doi.org/10.18517/ijaseit.12.5.14835

[56] A. B. Salsabila, B. N. Ruchjana, and A. S. Abdullah, "DEVELOPMENT OF THE GSTARIMA(1,1,1) MODEL ORDER FOR CLIMATE DATA FORECASTING," *Int. J. Data Netw. Sci.*, vol. 8, no. 2, pp. 773–788, 2024. doi: https://doi.org/10.5267/j.ijdns.2024.1.001

[57] A. Aprianti, N. Faulina, and M. Usman, "GENERALIZED SPACE TIME AUTOREGRESSIVE (GSTAR) MODEL FOR AIR TEMPERATURE FORECASTING IN THE SOUTH SUMATERA, RIAU, AND JAMBI PROVINCES," *Inpr. Indones. J. Pure Appl. Math.*, vol. 6, no. 1, pp. 1–13, 2024. doi: https://doi.org/10.15408/inprime.v6i1.36049

[58] M. Huda, N. Imro'ah, M. Y. Ayyash, and H. Pratiwi, "FOREST FIRES IN PEATLANDS ANALYZED FROM VARIOUS PERSPECTIVES : SPATIAL , TEMPORAL , AND SPATIAL-TEMPORAL," *J. Teor. dan Apl. Mat.*, vol. 9, no. 2, pp. 482–496, 2025. doi: https://doi.org/10.31764/jtam.v9i2.28884

[59] M. Y. Ayyash, M. Huda, and N. Imro, "THE GSTAR (1 ; 1) MODELLING WITH THREE COMBINATION OF THE GRID SIZES AND SPATIAL WEIGHT MATRIX IN FOREST FIRES CASES," *J. Teor. dan Apl. Mat.*, vol. 9, no. 1, pp. 134–146, 2025. doi: https://doi.org/10.31764/jtam.v9i1.27543

[60] C. F. Baum and S. Hurn, "'WHAT GOOD IS A VOLATILITY MODEL?' A REEXAMINATION AFTER 20 YEARS," *Stata J.*, vol. 21, no. 2, pp. 295–319, 2021. doi: https://doi.org/10.1177/1536867X211025797